AGU PUBLICATIONS

Geophysical Research Letters

RESEARCH LETTER
10.1002/2016GL072364

Key Points:
- Evaporation of secondary organic aerosol from α-pinene ozonolysis was studied under different relative humidity
- At dry conditions the evaporation was likely slowed down by diffusion limitations resulting from viscosity of the particles
- At atmospherically relevant relative humidity, diffusion limitations had a minor effect on evaporation of the particles

Supporting Information:
- Supporting Information S1
- Movie S1

Correspondence to:
T. Yli-Juuti,
taina.yli-juuti@uef.fi

Citation:
Yli-Juuti, T., et al. (2017), Factors controlling the evaporation of secondary organic aerosol from α-pinene ozonolysis, *Geophys. Res. Lett.*, *44*, 2562–2570, doi:10.1002/2016GL072364.

Received 14 SEP 2016
Accepted 22 FEB 2017
Accepted article online 25 FEB 2017
Published online 6 MAR 2017

Factors controlling the evaporation of secondary organic aerosol from α-pinene ozonolysis

Taina Yli-Juuti[1], Aki Pajunoja[1], Olli-Pekka Tikkanen[1], Angela Buchholz[1], Celia Faiola[1], Olli Väisänen[1], Liqing Hao[1], Eetu Kari[1], Otso Peräkylä[2], Olga Garmash[2], Manabu Shiraiwa[3], Mikael Ehn[2], Kari Lehtinen[1,4], and Annele Virtanen[1]

[1]Department of Applied Physics, University of Eastern Finland, Kuopio, Finland, [2]Department of Physics, University of Helsinki, Helsinki, Finland, [3]Department of Chemistry, University of California, Irvine, California, USA, [4]Finnish Meteorological Institute, Kuopio, Finland

Abstract Secondary organic aerosols (SOA) forms a major fraction of organic aerosols in the atmosphere. Knowledge of SOA properties that affect their dynamics in the atmosphere is needed for improving climate models. By combining experimental and modeling techniques, we investigated the factors controlling SOA evaporation under different humidity conditions. Our experiments support the conclusion of particle phase diffusivity limiting the evaporation under dry conditions. Viscosity of particles at dry conditions was estimated to increase several orders of magnitude during evaporation, up to 10^9 Pa s. However, at atmospherically relevant relative humidity and time scales, our results show that diffusion limitations may have a minor effect on evaporation of the studied α-pinene SOA particles. Based on previous studies and our model simulations, we suggest that, in warm environments dominated by biogenic emissions, the major uncertainty in models describing the SOA particle evaporation is related to the volatility of SOA constituents.

1. Introduction

Atmospheric aerosols play an important role in the climate system by scattering and absorbing solar radiation and by affecting cloud properties and lifetimes through their ability to act as cloud condensation nuclei [*Stocker et al.,* 2013]. Aerosols also deteriorate air quality causing decreased visibility and adverse health effects [*Dockery and Pope*, 1994]. A large fraction of atmospheric particulate material consists of secondary organic aerosol (SOA) which is formed when volatile organic compounds (VOCs) oxidize and form condensable trace gases [*Hallquist et al.,* 2009]. The volatile SOA precursor gases comprise emissions from both biogenic and anthropogenic sources, and their oxidation products include diverse compounds with a large variety in saturation concentrations, functional groups, and other properties [*Hallquist et al.,* 2009; *Goldstein and Galbally*, 2007; *Kroll and Seinfeld*, 2008]. The complexity and unknown properties of SOA set a great challenge for understanding atmospheric aerosol effects [*Kanakidou et al.,* 2005]. Dynamics of SOA systems are especially sensitive to compounds' properties such as volatility, chemical reactivity, and diffusivity.

To overcome the daunting complexity of atmospheric SOA, simplified approaches are used to represent the vast number of different organic compounds in models. One approach, widely used in SOA studies, is the volatility basis set (VBS) approach [*Donahue et al.,* 2006], which lumps the compounds based on their saturation concentration (C^*). It is typically applied together with equilibrium gas-particle partitioning theory [*Pankow*, 1994] for determining the particle and/or gas phase compositions of SOA systems with different precursor gases. Such approaches typically assume either instantaneous gas-particle equilibration and/or instantaneous mixing within the particle phase. In both cases they omit mass transport limitations inside particles and, often, also omit particle phase chemical transformations.

α-Pinene is among the main atmospheric SOA precursor VOCs, and the SOA derived from oxidation of α-pinene is often used as a replica of atmospheric SOA [*Hallquist et al.,* 2009]. Based on SOA growth studies, the volatility of SOA derived from α-pinene ozonolysis has a VBS with C^* between 10^{-2} and 10^4 μg m^{-3} [*Pathak et al.,* 2007]. In addition to the C^* of the SOA constituents, also the physical phase state of the SOA particles can affect their growth and evaporation. Within a viscous semisolid particle, the diffusion of molecules proceeds slower than in a liquid particle, which affects their ability to evaporate. *Vaden et al.* [2011] reported slower evaporation of α-pinene ozonolysis SOA under dry conditions compared to the expected evaporation rate based on the VBS parameterization derived from the SOA growth experiments.

Additionally, the anomalously slow evaporation rate did not exhibit similar size dependence as expected for vapor pressure-driven evaporation. It has been suggested that the slow evaporation is due to diffusional mass transport limitations in the particle phase arising from the viscous phase of the particles [*Vaden et al.,* 2011] or due to a combination of oligomer degradation and mass transfer limitations [*Roldin et al.,* 2014]. These hypotheses are supported by the unchanged composition of α-pinene SOA particles upon heating [*Cappa and Wilson*, 2011]. There is some variability in measured evaporation rates of α-pinene SOA depending on humidity conditions. *Wilson et al.* [2015] reported faster evaporation for SOA particles from α-pinene ozonolysis at 90% relative humidity (RH) compared to RH < 5% and at 50% RH they observed evaporation kinetics similar to the low RH conditions. The reduced diffusivity within the particles, and consequently, slower evaporation rate, as the RH decreases is consistent with particle viscosity measurements that report α-pinene SOA viscosities ranging from those of semisolid or solid material to liquid over the RH range up to 90% [*Rembaum-Wolff et al.,* 2013; *Zhang et al.,* 2015]. Also, a decrease in the bouncing of α-pinene SOA particles with increasing RH indicates changes in particles' viscosity [*Kidd et al.,* 2014; *Pajunoja et al.,* 2015]. The bouncing of freshly formed atmospheric secondary particles suggests that the viscosity observations of α-pinene SOA have atmospheric relevance, at least in the boreal forest environment [*Virtanen et al.,* 2010].

Mass transfer limitations have been the primary explanation for slow particle evaporation rates, but there are other possibilities. Uncertainty in the VBS parameterizations may also affect the interpretation of the SOA evaporation experiments. The slow evaporation could be consistent with α-pinene SOA that contains compounds with lower C^* than what is reported in the previous VBS studies. In fact, highly oxidized, and likely very low-volatile, organics have been observed in the gas phase both in laboratory-generated α-pinene SOA systems and in the atmosphere [*Ehn et al.,* 2014; *Jokinen et al.,* 2015]. Such low-volatile compounds are not represented in existing VBS parameterizations which are derived from SOA growth chamber experiments where organic aerosol mass loadings are orders of magnitude higher than the C^* of these compounds. These newly identified compounds have not been included in detailed gas chemical models [*Roldin et al.,* 2014]. Further, vapor losses on the chambers' walls would be amplified for lower-volatility compounds and would distort laboratory-derived VBS toward higher volatilities if not accounted for appropriately [*Kokkola et al.,* 2014; *McVay et al.,* 2014; *Matsunaga and Ziemann*, 2010].

In this study, we explore the roles of both volatility and viscosity in determining evaporation rates of α-pinene ozonolysis SOA particles under both dry and atmospherically relevant humidity conditions. The measured data are interpreted using an evaporation model with a description of particle phase diffusion in order to determine the role of diffusion limitations at atmospherically relevant RH and timescales. Our results in dry conditions are consistent with previous studies [*Vaden et al.,* 2011; *Wilson et al.,* 2015] and support the conclusion of particle phase diffusivity limiting the evaporation. In contrast, at atmospherically relevant RH and time scales, our results demonstrate that the diffusion limitations have a minor effect on evaporation of α-pinene SOA particles.

2. Materials and Methods

2.1. Measurements

SOA was formed by ozone oxidation of α-pinene in a continuous flow tube reactor at dry condition. Exception was one dry evaporation experiment where particles were formed at 30% RH. The used relative humidities (RHs) inside the flow tube did not affect the evaporation rate. Mixing ratios of α-pinene and ozone at the flow tube inlet were 500–800 ppb and 600 ppb, respectively. Approximately 200 ppb of α-pinene reacted. The O:C of the SOA, which describes the degree of oxidation, was 0.55 corresponding well with values reported for fresh SOA in a monoterpene-rich environment [*Pennington et al.,* 2013]. The aerosol was led through an ozone scrubber, and then a monodisperse particle population was selected with a differential mobility analyzer (DMA) using clean air as sheath air. The DMA was operated in an open loop configuration in order to dilute the remaining gas phase compounds. The DMA flows and the short tube length ensured that the mixing of the sheath and sample flows were minimal resulting in high dilution ratios at the outlet of the DMA driving the particle evaporation [*Li and Chen*, 2005]. The size selected (mobility diameter 80 nm) particle population was led to a clean 100 L polished stainless steel chamber until particles were detected at the outlet (approximately 30–60 min filling time), after which the chamber was closed. Short residence time data (2–130 s) were obtained when the evaporation chamber was bypassed, and instead, the SOA was sampled

after size selection through varying lengths of stainless steel tubing. Intermediate residence time data (~30 min) were obtained by sampling at the end of the evaporation chamber during filling. At various times throughout the experiment, sampling from the evaporation chamber was resumed for approximately 20 min. This method was repeated providing long residence time data for each evaporation experiment (2–4 h). All experiments were performed at room temperature. The sample (at the DMA) and the evaporation chamber humidities were conditioned either with dry air or with air humidified to 40% or 80% RH. Particle size was measured at each sampling point.

Particle number size distribution was measured with a scanning mobility particle sizer. Particle composition was measured with an Aerodyne High-Resolution Time-of-Fight Aerosol Mass Spectrometer (hereafter AMS) [*DeCarlo et al.,* 2006; *Aiken et al.,* 2007; *Canagarathan et al.,* 2015]. α-pinene gas phase concentration was measured with a Proton Transfer Reaction Time-of-Flight Mass Spectrometer. The measurement setup is described in detail in Text S1 in the supporting information.

2.2. Modeling

The measured particle evaporation was analyzed using two evaporation models for a monodisperse particle population. One model was based on evaporation mass flux due to gas phase diffusion and assumes a well-mixed liquid-like particle phase [*Vesala et al.,* 1997; *Lehtinen and Kulmala*, 2003]. The other was a kinetic multilayer model KM-GAP [*Shiraiwa et al.,* 2012; *Shiraiwa et al.,* 2013], which allows investigation of particle phase mass transport. Models were initialized with the measured particle size at the DMA and an assumption of the initial particle composition. The organic compounds were represented with a 1-D VBS [*Donahue et al.,* 2006] using eight C^* bins with decadal difference between 10^{-3} and 10^{4} μg m^{-3}. All organic compounds were assumed to have molar mass of 150 g mol^{-1}, gas phase diffusivity of 0.058 cm^2 s^{-1}, density of 1.2 g cm^{-3}, mass accommodation coefficient of 1, and desorption lifetime of 10^{-6} s. Simulations were performed at 298.15 K. In simulations for humid conditions, water was assumed to constantly reach instantaneous gas-particle surface equilibrium, and the aqueous solution was assumed ideal for calculating water molar fraction. Use of measured hygroscopic growth factors instead of the ideal solution assumption was also tested for the liquid-like model (see supporting information). Unless otherwise stated, an instantaneous complete wall loss was assumed for the evaporated vapors (see supporting information).

The initial particle composition was optimized with the well-mixed particle evaporation model using a genetic algorithm [*Goldberg,* 1989] to determine a VBS that would reproduce observed evaporation rates. We ran 20 genetic algorithm simulations resulting into 20 different initial particle volatility basis sets (VBSs) that captured the observed evaporation well. Among these 20 cases the one with best fitness was selected as the best fit composition. During the fitting procedure, initial volatility distributions that suggested unreasonably high oxidized organic mass compared to reacted α-pinene mass in the flow tube were disregarded (see supporting information). This restriction affected mainly to the highest C^* bin. As reacted α-pinene mass was used only as an upper limit for organic mass, the resulted VBSs were not sensitive for vapor wall losses in the flow tube.

The multilayer model was modified from the KM-GAP model by allowing for the surface layer to combine with the outermost bulk layer when the surface layer thickness has reduced to < 0.5 nm. This was required for modeling the multicomponent system without seed particles or nonvolatile compounds. Composition dependence of particle viscosity (η) was assumed to have the form

$$\log_{10}(\eta) = \sum_i X_i \log_{10}(b_i) \quad (1)$$

where X_i is the dry particle molar fraction of the volatility bin i and b_i is a coefficient that describes the effect of bin i on the viscosity [*O'Meara et al.,* 2016]. Values of b_i were varied independently for dry and 40% RH conditions to find matches between model simulations and measurements. The particle phase diffusivities were calculated based on the viscosity using the Stokes-Einstein relation. The particle phase diffusivities were equal for all organic compounds as we assigned equal molar masses for them.

3. Results

The particle evaporation at each RH was considerably slower than expected based on the VBS previously determined for α-pinene dry ozonolysis SOA from growth experiments [*Pathak et al.,* 2007] and assuming

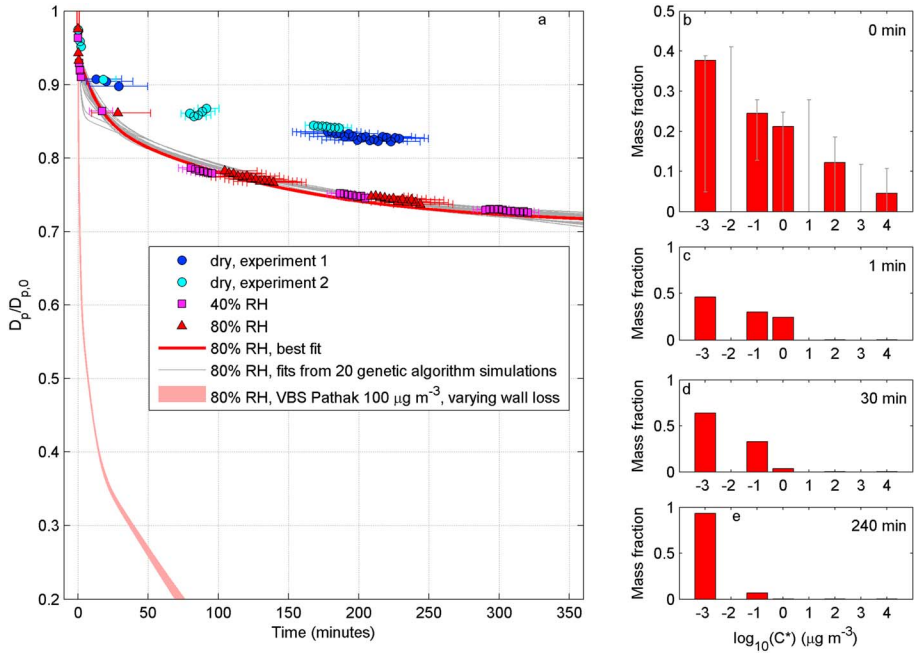

Figure 1. Measured evaporation of particles with initial size 80 nm and model simulations at 80% RH. (a) Time evolution of particle diameter normalized with the initial diameter. Markers show measured evaporation under different humidity. The error bars in time originate from the chamber filling time. Well-mixed particle model simulations at 80% RH: Size evolution with the best fit initial volatility distribution for 80% RH (red line in Figure 1a), and size evolution for the best fits from 20 genetic algorithm simulations (gray lines in Figure 1a). Size evolution with the initial volatility distribution calculated based on the flow tube mass loading and the *Pathak et al.* [2007] VBS parameterization and assuming varying vapor wall loss rate from complete instantaneous wall loss to no wall loss (light red shaded area in Figure 1a). (b-e) Best fit initial particle volatility distribution for 80% RH and the evolution of particle composition. Variability in the initial volatility distribution (minimum and maximum as error bars) within the 20 genetic algorithm simulations is also shown in Figure 1b.

perfectly mixed liquid particles (Figure 1a). In addition, the measurements clearly show that particles evaporated faster at humid conditions (40% and 80% RH) compared to dry conditions (Figure 1a). The observations of slow evaporation under all humidity conditions and the slower evaporation under dry conditions compared to high RH (80%) are consistent with previous studies, where particles were formed in a Teflon bag and their evaporation was measured in a separate chamber [*Vaden et al.,* 2011; *Wilson et al.,* 2015]. Interestingly, in our case the evaporation at 40% RH was similar to 80% RH, while *Wilson et al.* [2015] observed similar evaporation kinetics at 50% RH compared to dry conditions. The reason for this difference between the studies at moderate RH may be due to different SOA formation conditions: *Wilson et al.* [2015] used a Teflon chamber with an OH scavenger, while our experiments were conducted in a flow tube without an OH scavenger. These different oxidation conditions may have led to different particle composition. The overall evaporation rates of the 80 nm particles in our study were close to those observed previously for 125–414 nm particles [*Vaden et al.,* 2011; *Wilson et al.,* 2015] (Figure S4).

Based on current literature, it can be assumed that α-pinene SOA particles have relatively low viscosity at 80% RH [*Rembaum-Wolff et al.,* 2013] and higher viscosity at dry conditions (RH ~ 0%) [*Zhang et al.,* 2015]. Hence, we started our model simulations from the 80% RH where we can assume that the diffusion timescales in particle bulk were short compared to the gas phase and that the "traditional" evaporation model assuming fully mixed liquid-like particles was valid for simulating the evaporation. Results shown later demonstrate that the assumption is valid up to viscosity values as high as 10^4–10^5 Pa s. It should be noted that the evaporation modeling is sensitive to the treatment of vapor wall losses when particle number concentration is high. To qualitatively resolve the best treatment for wall losses in our system, we performed two experiments at dry conditions with particle number concentrations differing by approximately an order of magnitude. The evaporation rate was similar for both cases (Figure 1a) indicating that the vapor wall loss rates were fast, faster than approximately 10^{-2} s^{-1}, and that the instantaneous wall loss assumption in the model was reasonable (Figure S2).

We modeled the evaporation at 80% RH by optimizing the VBS at the beginning of the evaporation so that the model matched the measured evaporation curve (red curve in Figure 1 and red bars in Figure 1b). This optimized VBS is referred to as the "initial VBS" hereon. With eight C^* bins the experimental curve can be reproduced almost perfectly with several different initial volatility distributions (Figures 1a and 1b; see supporting information). The sensitivity to the initial mass fractions of the bins with $C^* \geq 10^0\ \mu g\ m^{-3}$ was especially low. The simulations, however, clearly demonstrated that a considerable fraction (>36%) of mass was needed in the two least volatile bins of the VBS ($C^* \leq 10^{-2}\ \mu g\ m^{-3}$) to replicate the experimental results at 80% RH (Figure 1b). These two volatility bins are the main contributors in the particle phase at the end of the evaporation experiment (Figure 1e; see Movie S1 representing the evolution of particle phase composition). As the C^* range extended down to only $10^{-3}\ \mu g\ m^{-3}$, this bin includes all compounds with $C^* \leq 10^{-3}\ \mu g\ m^{-3}$, i.e., compounds with low volatility relative to the experiment time scale. Also of particular note is that a large fraction (>25%) of the mass was required to be initially in the C^* bins of 10^{-1}–$10^0\ \mu g\ m^{-3}$.

The evaporation rate was clearly lower at dry conditions compared to humid conditions (Figure 1). The particles were generated in similar conditions in the flow tube in all three humidity cases shown in Figure 1, and therefore, drastically different initial organic compositions between the dry and the wet experiments were unlikely. The observed differences in evaporation rates between dry and humid conditions cannot be explained by Raoult's effect resulting from the water uptake at elevated RHs because the solution effect would slow down the evaporation of wet particles compared to dry particles. The difference in evaporation rates between dry and wet conditions could be due to two factors: (1) The particle phase diffusional limitations slow down the evaporation of the semisolid dry particles as suggested by *Vaden et al.* [2011] and/or (2) particle phase chemical reactions take place in the evaporating particles changing the volatility of their constituents. In the latter case the presence of water should either catalyze reactions that increase the volatility (e.g., fragmentation) or inhibit reactions that lower the volatility (e.g., oligomerization). We analyzed the data from dry and 40% RH experiments according to these two scenarios and present the results below.

To investigate the role of particle phase state in the evaporation process of SOA, and to define the viscosity of the evaporating particles, we focused first on the experiments conducted under dry conditions, where particle phase influences would be the highest. This was done by simulating the evaporation with a multilayer evaporation model including a description of particle phase diffusion. The composition of the particles was represented in the model with the initial VBS determined from the 80% RH experiment. The initial VBS corresponds to the composition at the DMA, and until there the particles had been under same conditions in each experiment. To capture the shape of the dry evaporation curve required a strong composition dependence in the particles' viscosity, with viscosity values varying approximately from 10^5 Pa s to 10^9 Pa s as the evaporation occurred (Figures 2a and 2c). These values are comparable with published viscosity values for α-pinene SOA considering the associated large uncertainties [*Rembaum-Wolff et al.,* 2013; *Zhang et al.,* 2015]. Particle evaporation and changing composition during earlier viscosity measurements is highly possible complicating direct comparison of the results. The increase in viscosity as the particle evaporates and the particle composition shifts toward lower volatility is in agreement with the recent study, which reported lower viscosity when α-pinene SOA was formed under high mass concentration compared to lower mass concentration conditions [*Grayson et al.*, 2016].

Our results indicate that the least volatile constituents remaining at the end of the evaporation have a larger molar mass resulting in increased viscosity [*Koop et al.,* 2011]. According to our simulations assuming constant viscosity, the particle phase diffusivity already limits the early evaporation period (i.e., first few minutes) with particle viscosity of 10^5 Pa s. The overall evaporation behavior (e.g., the shape of the curve) is affected considerably when the viscosity is higher than 10^6 Pa s (compare blue and green dashed lines to the red dashed line in Figure 2a). It should be noted that our model calculations provide only an order of magnitude estimate of the particle viscosity, although the model predictions are sensitive to the choice of viscosity. This is because there are relatively large uncertainties in the mass fractions of the highest-volatility bins at the beginning of the evaporation.

Particle evaporation at 40% and 80% RH were almost identical, with the 40% RH experiment showing slightly faster evaporation at the beginning (Figure 2b). Due to Raoult's effect, a clearly faster evaporation at 40% compared to 80% RH is expected for well-mixed solution droplets having the same initial organic

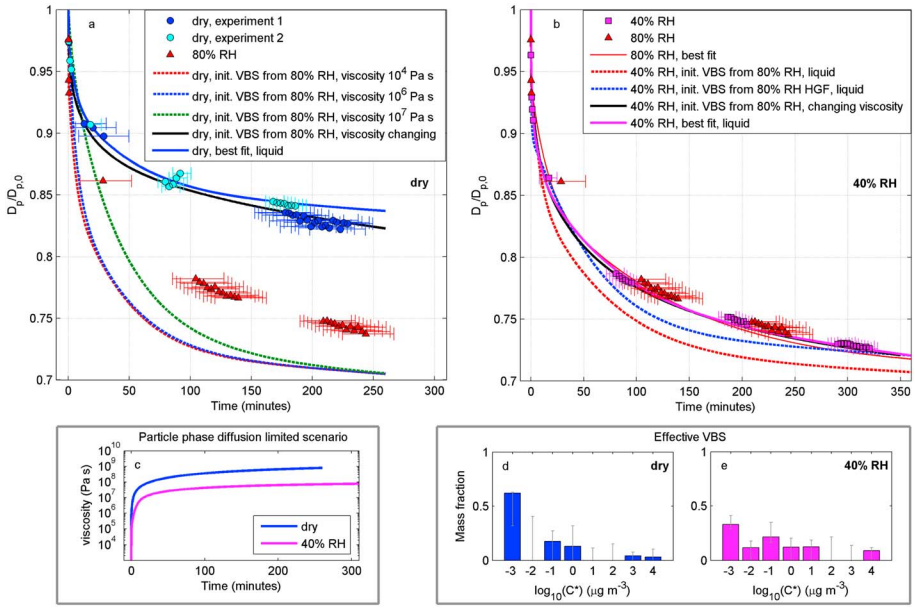

Figure 2. Model simulations for evaporation of particles with initial size 80 nm under dry and 40% RH conditions. Time evolution of particle diameter normalized with the initial diameter (Figures 2a and 2b). Markers show measured evaporation under different humidity. The error bars in time originate from the chamber filling time. (a) Simulations for dry conditions: multilayer model using the initial VBS from the 80% RH experiment and assuming constant (dashed lines) or a composition-dependent particle viscosity (black line) and well-mixed particle model with the best fit initial composition for the dry 2 experiment (blue solid line). (b) Simulations for 40% RH: well-mixed particle model with the initial VBS from 80% RH assuming an ideal solution (red dashed line) and with water uptake calculated based on HGF (blue dashed line; see Figure S3), multilayer model with the initial VBS from 80% RH and assuming a composition-dependent particle viscosity (black line) and well-mixed particle model simulation with the best fit initial composition at 40% RH. (c) Particle viscosities correspond to the model simulations shown with black lines in Figures 2a and 2b. Effective VBSs show the best fit initial VBS (bars) and variability within 20 genetic algorithm simulations (error bars) from the optimization of the well-mixed particle model for (d) the dry and (e) 40% RH cases.

composition with different water mole fractions, as demonstrated in Figure 2b. The unexpectedly small difference in the evaporation rates between 40% and 80% RH may be related to diffusion limitations at 40% RH or to uncertainties in calculating water uptake of α-pinene SOA in the model and/or experiments. The basic version of the model calculated particle water content assuming an ideal solution. To study the uncertainty concerning the water uptake description, model simulations were also performed using experimentally determined hygroscopic growth factors (HGF) of α-pinene SOA at 80% RH (HGF = 1.05) and 40% RH (HGF = 1.01) [*Pajunoja et al.,* 2015; *Varutbangkul et al.,* 2006]. The experimentally determined HGF predict a smaller difference in evaporation between the two RH cases compared to the ideal solution assumption and bring the simulation results at 40% RH closer to the observations (blue dashed line in Figure 2b; see also Figure S3). Still, even with the experimental HGF the well-mixed particle evaporation model predicts slightly faster evaporation than observed at 40% RH. However, the predicted differences in evaporation rates between 40% and 80% RH are rather small, and we cannot eliminate the possibility that the deviation between measured and simulated evaporation rates at 40% RH is due to experimental uncertainties.

To study the possible effect of particle phase diffusion limitations at 40% RH, we used the VBS determined at 80% RH and simulated the evaporation at 40% RH with the multilayer evaporation model. Similar to the dry condition, reproducing the observed slowing evaporation at 40% RH with the model required an increase in viscosity as evaporation proceeded, with values reaching approximately 10^8 Pa s (Figures 2b and 2c). The required viscosity values are in agreement with previously published values for α-pinene SOA [*Rembaum-Wolff et al.,* 2013; *Zhang et al.,* 2015] and notably are approximately an order of magnitude lower than in the dry condition. As 40% RH represents the lower end of typical humidity in the atmospheric boundary layer, our results suggest that particle phase diffusion limitations in the evaporation of α-pinene type SOA are possible in drier atmospheric conditions. However, the effect may be small even if the

viscosity values are relatively high at the end of the evaporation where only low vapor pressure compounds remain in the particle phase.

In our approach the optimization of the initial VBS gives an "effective VBS." We make this distinction because the evaporation could also be affected significantly by chemical reactions that are dependent on water content and could influence SOA composition and volatility, such as oligomer decomposition rates. The chemistry of oligomer decomposition was not simulated in our model. However, the effective VBS is fit to the observations and thus includes any effects on the evaporation rate controlled by oligomer decomposition rates which would influence compound volatility. Although, it should be noted that the effective VBS does not provide any information about the decomposition processes itself; it only provides information on the initial volatility distribution required to reproduce the measurements. We repeated the analysis from the 80% RH (assuming well-mixed particles) with data from the dry and the 40% RH experiment to compare the effective VBSs (Figures 2d and 2e). The resulting effective VBS at dry conditions showed a shift of mass toward the lowest two volatility bins (>61% by mass in the bins $C^* \leq 10^{-2}\,\mu g\,m^{-3}$) (Figure 2d) compared to the 80% RH case. For 40% RH the difference compared to 80% RH was less pronounced (Figure 2e). Such differences in the effective VBS derived at varying RH could be explained by increase in oligomer decomposition rate with RH. The effective VBS derived at dry conditions (Figure 2e) qualitatively agrees with the VBS derived from the previous dry condition evaporation experiments [*Shrivastava et al.,* 2013] although quantitative differences exist in accordance with the somewhat faster evaporation in the previous experiments [*Vaden et al.,* 2011].

4. Discussion

Simulation of SOA particle evaporation based on a VBS previously determined from SOA growth experiments failed to capture the size evolution of both wet and dry particles. Instead, a volatility distribution with mass shifted toward lower volatility was required to capture the evaporation. This result is consistent with recently reported atmospheric and laboratory observations of condensable low-volatile organic compounds in the gas phase [*Ehn et al.,* 2014; *Jokinen et al.,* 2015]. Interestingly, the O:C of the evaporating particles was constant throughout the evaporation process (approximately 0.55) suggesting that the variation of O:C between VBS bins was small. Such a constant and relatively low O:C is not expected if the compounds in the least volatile VBS bins—whose relative abundance in the particles increases as the evaporation proceeds—had clearly higher O:C than the more volatile constituents. Instead, we hypothesize that the low-volatile compounds were oligomers, having O:C values comparable to more volatile monomers. Such dimers have been detected in α-pinene ozonolysis [*Ehn et al.,* 2014; *Kristensen et al.,* 2014]. This is also in agreement with the model results showing increase in particle viscosity with proceeding evaporation. The constant O:C ratio is consistent with the unchanged mass spectra of α-pinene SOA upon heating reported by *Cappa and Wilson* [2011], who hypothesized this to be either due to diffusion limitations within the particle phase causing the evaporation to proceed layer by layer or due to high particle mass fraction consisting of oligomers whose decomposition controls the evaporation.

In the lowest RH condition, our results demonstrating that particle evaporation is influenced by viscosity effects are in agreement with a previous study by *Vaden et al.* [2011]. We cannot rule out the possibility that particle phase chemical reactions, such as oligomer decomposition, are also limiting the evaporation. In this case, to explain our experimental observations, particle phase water should accelerate reactions that lead to more volatile composition. Such reactions relate to changes in the effective VBS as comparison of our results at dry and 80% RH conditions demonstrate.

At 40% RH that represents the lower limit of atmospheric humidity, our results are contrary to *Wilson et al.* [2015] findings. This difference between studies suggests that factors limiting particle evaporation are sensitive to the conditions and thus highlights challenges in applying laboratory results to simulations and interpretations of atmospheric SOA. For example, the fraction of semivolatiles in particles at the beginning of the evaporation may depend on SOA generation methodology (e.g., organic mass loading) and also on sample treatment prior to size detection. The semivolatiles evaporate during the first few minutes, so their particle mass fraction affects the overall evaporation rate and measured shape of the evaporation curve. In the flow tube experiments the organic mass loadings are higher and particle composition is likely shifted toward higher volatility compared to typical atmospheric conditions. Evaporation of the more volatile

compounds is likely more prone to exhibit particle phase diffusivity effects upon evaporation as their evaporation time scales are shorter compared to less volatile compounds. Recognizing limitations of laboratory experiments, we still highlight that our SOA had O:C comparable to monoterpene-rich environments. While further investigation of particle viscosity at the lower limit of atmospheric RH is still necessary, our results suggest that integrating the viscosity effect into regional or global models would be of less importance for improving SOA evaporation descriptions in warm, biogenic-dominated environments when considering (1) the sensitivity of particles' evaporation rates to assumed VBS distribution and (2) the uncertainties in the current VBS descriptions, particularly regarding recently measured low volatility compounds [*Ehn et al.,* 2014] which have not been taken into account. In addition, considering recent results showing that atmospheric organic aerosols are liquid in most cases in a pristine Amazonian environment and also in an isoprene and terpene rich environment in southeast U.S. [*Bateman et al.,* 2016; *Pajunoja et al.,* 2016], we conclude that higher scientific priority for future investigations is to decrease uncertainties in VBS representations of the organic compounds contributing to SOA production.

Acknowledgments
This work was supported by the Academy of Finland (272041, 259005, and 299544), European Research Council (ERC starting grants 335478 and 638703), and the strategic funding from University of Eastern Finland. The data may be obtained from the corresponding author upon request.

References

Aiken, A. C., P. F. DeCarlo, and J. L. Jimenez (2007), Elemental analysis of organic species with electron ionization high-resolution mass spectrometry, *Anal. Chem.*, *79*, 8350–8358.

Bateman, A., et al. (2016), Sub-micrometre particulate matter is primarily in liquid form over Amazon rainforest, *Nat. Geosci.*, *9*, 34–37.

Canagarathan, M. R., et al. (2015), Elemental ratio measurements of organic compounds using aerosol mass spectrometry: Characterization, improved calibration, and implications, *Atmos. Chem. Phys.*, *15*, 253–272.

Cappa, C. D., and K. R. Wilson (2011), Evolution of organic aerosol mass spectra upon heating: Implications for OA phase and partitioning behavior, *Atmos. Chem. Phys.*, *11*, 1895–1911.

DeCarlo, P. F., et al. (2006), Field-deployable, high-resolution, time-of-flight aerosol mass spectrometer, *Anal. Chem.*, *78*, 8281–8289.

Dockery, D., and C. Pope (1994), Acute respiratory effects of particulate air-pollution, *Annu. Rev. Publ. Health*, *78*(24), 107–132.

Donahue, N., A. Robinson, C. Stanier, and S. Pandis (2006), Coupled partitioning, dilution, and chemical aging of semivolatile organics, *Environ. Sci. Technol.*, *40*(8), 2635–2643.

Ehn, M., et al. (2014), A large source of low-volatility secondary organic aerosol, *Nature*, *506*, 476–479.

Goldberg, D. E. (1989), *Genetic Algorithms in Search, Optimization and Machine Learning*, Addison-Wesley, Boston, Mass.

Goldstein, A. H., and I. E. Galbally (2007), Known and unexplored organic constituents in the Earth's atmosphere, *Environ. Sci. Technol.*, *41*(5), 1514–1521.

Grayson, J. W., Y. Zhang, A. Mutzel, L. Renbaum-Wolff, O. Böge, S. Kamal, H. Herrmann, S. T. Martin, and A. k. Bertram (2016), Effect of varying experimental conditions on the viscosity of α-pinene derived secondary organic material, *Atmos. Chem. Phys.*, *16*, 6027–6040.

Hallquist, M., et al. (2009), The formation, properties and impact of secondary organic aerosol: Current and emerging issues, *Atmos. Chem. Phys.*, *9*(14), 5155–5236.

Jokinen, T., et al. (2015), Production of extremely low volatile organic compounds from biogenic emissions: Measured yields and atmospheric implications, *Proc. Natl. Acad. Sci. U.S.A.*, *112*(23), 7123–7128.

Kanakidou, M., et al. (2005), Organic aerosol and global climate modelling: A review, *Atmos. Chem. Phys.*, *5*, 1053–1123.

Kidd, C., V. Perraud, L. M. Wingen, and B. J. Finlayson-Pitts (2014), Integrating phase and composition of secondary organic aerosol from the ozonolysis of α-pinene, *Proc. Natl. Acad. Sci. U.S.A.*, *111*(21), 7552–7557.

Kokkola, H., et al. (2014), The role of low volatile organics on secondary organic aerosol formation, *Atmos. Chem. Phys.*, *14*, 1689–1700.

Koop, T., J. Bookhold, M. Shiraiwa, and U. Pöschl (2011), Glass transition and phase state of organic compounds: Dependency on molecular properties and implications for secondary organic aerosols in the atmosphere, *Phys. Chem. Chem. Phys.*, *13*, 19,238–19,255.

Kristensen, K., T. Cui, H. Zhang, A. Gold, M. Glasius, and J. D. Surratt (2014), Dimers in α-pinene secondary organic aerosol: Effect of hydroxyl radical, ozone, relative humidity and aerosol acidity, *Atmos. Chem. Phys.*, *14*, 4201–4218.

Kroll, J. H., and J. H. Seinfeld (2008), Chemistry of secondary organic aerosol: Formation and evolution of low-volatility organics in the atmosphere, *Atmos. Environ.*, *42*(16), 3593–3624.

Lehtinen, K. E. J., and M. Kulmala (2003), A model for particle formation and growth in the atmosphere with molecular resolution in size, *Atmos. Chem. Phys.*, *3*, 251–257.

Li, W., and D.-R. Chen (2005), Performance of nano-DMA operated with different gases for sheath and aerosol carrier flows, *Aerosol Sci. Technol.*, *39*, 931–940.

Matsunaga, A., and P. Ziemann (2010), Gas-wall partitioning of organic compounds in a Teflon film chamber and potential effects on reaction product and aerosol yield measurements, *Aerosol Sci. Technol.*, *44*, 881–892.

McVay, R. C., C. D. Cappa, and J. H. Seinfeld (2014), Vapor-wall deposition in chambers: Theoretical considerations, *Environ. Sci. Technol.*, *48*, 10,251–10,258.

O'Meara, S., D. O. Topping, and G. McFiggans (2016), The rate of equilibration of viscous aerosol particles, *Atmos. Chem. Phys.*, *16*, 5299–5313.

Pajunoja, A., et al. (2015), Adsorptive uptake of water by semisolid secondary organic aerosols, *Geophys. Res. Lett.*, *42*, 3063–3068, doi:10.1002/2015GL063142.

Pajunoja, A., W. Hu, Y. J. Leong, N. F. Taylor, P. Miettinen, B. B. Palm, S. Mikkonen, D. R. Collins, J. L. Jimenez, and A. Virtanen (2016), Phase state of ambient aerosol linked with water uptake and chemical aging in the southeastern US, *Atmos. Chem. Phys.*, *16*, 11,163–11,176.

Pankow, J. F. (1994), An absorption model of gas/particle partitioning of organic compounds in the atmosphere, *Atmos. Environ.*, *28*(2), 185–188.

Pathak, R. K., A. A. Presto, T. E. Lane, C. O. Stanier, N. M. Donahue, and S. N. Pandis (2007), Ozonolysis of α-pinene: Parameterization of secondary organic aerosol mass fraction, *Atmos. Chem. Phys.*, *7*, 3811–3821.

Pennington, M. R., B. R. Bzdek, J. W. DePalma, J. N. Smith, A.-M. Kortelainen, L. Hildebrandt Ruiz, T. Petäjä, M. Kulmala, D. R. Worsnop, and M. V. Johnston (2013), Identification and quantification of particle growth channels during new particle formation, *Atmos. Chem. Phys.*, *13*, 10,215–10,225.

Rembaum-Wolff, L., J. W. Grayson, A. P. Bateman, M. Kuwata, M. Sellier, B. J. Murray, J. E. Shilling, S. T. Martin, and A. K. Bertram (2013), Viscosity of α-pinene secondary organic material and implications for particle growth and reactivity, *Proc. Natl. Acad. Sci. U.S.A.*, *110*(20), 8014–8019.

Roldin, P., et al. (2014), Modelling non-equilibrium secondary organic aerosol formation and evaporation with the aerosol dynamics, gas- and particle-phase chemistry kinetic multilayer model ADCHAM, *Atmos. Chem. Phys.*, *14*, 7953–7993.

Shiraiwa, M., C. Pfrang, T. Koop, and U. Pöschl (2012), Kinetic multi-layer model of gas-particle interactions in aerosols and clouds (KM-GAP): Linking condensation, evaporation and chemical reactions of organics, oxidants and water, *Atmos. Chem. Phys.*, *12*, 2777–2794.

Shiraiwa, M., L. D. Yee, K. A. Schilling, C. L. Loza, J. S. Craven, A. Zuend, P. J. Ziemann, and J. H. Seinfeld (2013), Size distribution dynamics reveal particle-phase chemistry in organic aerosol formation, *Proc. Natl. Acad. Sci. U.S.A.*, *110*(29), 11,746–11,750.

Shrivastava, M., A. Zelenyuk, D. Imre, R. Easter, J. Beranek, R. A. Zaveri, and J. Fast (2013), Implications of low volatility SOA and gas-phase fragmentation reactions on SOA loadings and their spatial and temporal evolution in the atmosphere, *J. Geophys. Res. Atmos.*, *118*, 3328–3342.

Stocker, T. F., et al. (2013), *Climate Change 2013, Physical Science Basis*, Cambridge Univ. Press, Cambridge, U. K., and New York.

Vaden, T. D., D. Imre, J. Beránek, M. Shrivastava, and A. Zelenyuk (2011), Evaporation kinetics and phase of laboratory and ambient secondary organic aerosol, *Proc. Natl. Acad. Sci. U.S.A.*, *108*(6), 2190–2195.

Varutbangkul, V., F. J. Brechtel, R. Bahreini, N. L. Ng, M. D. Keywood, J. H. Kroll, R. C. Flagan, J. H. Seinfeld, A. Lee, and A. H. Goldstein (2006), Hygroscopicity of secondary organic aerosols formed by oxidation of cycloalkenes, monoterpenes, sesquiterpenes, and related compounds, *Atmos. Chem. Phys.*, *6*, 2367–2388.

Vesala, T., M. Kulmala, R. Rudolf, A. Vrtala, and P. E. Wagner (1997), Model for condensational growth and evaporation of binary aerosol particles, *J. Aerosol Sci.*, *28*(4), 565–598.

Virtanen, A., et al. (2010), An amorphous solid state of biogenic secondary organic aerosol particles, *Nature*, *467*, 824–827.

Wilson, J., D. Imre, J. Beránek, M. Shrivastava, and A. Zelenyuk (2015), Evaporation kinetics of laboratory-generated secondary organic aerosols at elevated relative humidity, *Environ. Sci. Technol.*, *49*, 243–249.

Zhang, Y., et al. (2015), Changing shapes and implied viscosities of suspended submicron particles, *Atmos. Chem. Phys.*, *15*, 7819–7829.